Analysis of an all-in-plane spin-torque oscillator using injection locking to an external microwave magnetic field

*Hirofumi Suto[1], Hossein Sepehri-Amin[2], Nagarjuna Asam[2], Weinan Zhou[2], Anton Bolyachkin[2], Masayuki Takagishi[1], Naoyuki Narita[1], Shingo Tamaru[3], Tomoya Nakatani[2], and Yuya Sakuraba[2]

[1]*Corporate Research and Development Center, Toshiba Corporation, Kawasaki, 212-8582, Japan*

[2]*Research Center for Magnetic and Spintronic Materials, National Institute for Materials Science (NIMS), Tsukuba, 305-0047, Japan*

[3]*National Institute of Advanced Industrial Science and Technology (AIST), Research Center for Emerging Computing Technologies, Tsukuba, Ibaraki 305-8568, Japan*

*corresponding author (E-mail: hirofumi.suto@toshiba.co.jp)

ABSTRACT

We experimentally study the magnetization dynamics of an all-in-plane spin-torque oscillator (AIP-STO) by using injection locking to an external microwave magnetic field. The AIP-STO exhibits multiple frequency signals corresponding not only to the oscillation frequencies of the magnetic layers but also to the difference between these frequencies. The oscillation frequency is identified based on the principle that injection locking occurs only to the signal corresponding to the magnetization oscillation. We also analyze the magnetization dynamics during injection locking by micromagnetic simulations. The results demonstrate that injection locking is a powerful tool for elucidating the oscillation of the AIP-STO.

Microwave-assisted magnetic recording (MAMR) has attracted attention as a technology for hard disk drives (HDDs) that can overcome the limitations imposed by the writability problem of the conventional recording and deliver the continuous growth of recording density [1]–[6]. Key to implementing MAMR is the development of a spin-torque oscillator (STO) that can emit a microwave (MW) magnetic field with a frequency of a few tens of GHz [6]–[8]. An all-in-plane (AIP) STO, which typically consists of two in-plane magnetic layers: a field generation layer (FGL) and a spin injection layer (SIL) with a spacer between them, has been proposed as a promising STO design for MAMR application because of the following advantages [9]–[12]. Out-of-plane magnetization oscillation with a large cone angle is induced, which can generate a large-amplitude MW field. The structure is thin enough to fit in the narrow write gap of an HDD write head with a typical width of 20 nm. The onset of the oscillation is fast enough to achieve fast writing [9].

The oscillation frequency of FGL is an important parameter in MAMR which greatly affects the MAMR efficiency. Conventionally, the oscillation frequency has been estimated by measuring a high-frequency electrical signal (STO signal) originating from the resistance change due to the magnetoresistance (MR) effect. However, the STO signal from the AIP-STO exhibits multiple peaks corresponding not only to the oscillation of FGL, but also to that of SIL and the difference between these frequencies because magnetization dynamics are induced in both SIL and FGL. Although the multiple peaks can be explained by simulations [10], an experimental technique capable of analyzing the complex STO signal is desired.

In this work, we study the magnetization dynamics of an AIP-STO by using injection locking to an external MW magnetic field (H_{MW}). Injection locking is a phenomenon by which the STO magnetization synchronizes with an external driving force such as a magnetic field. Injection locking has been utilized to study in-plane magnetization oscillation [13]. By employing this technique, the AIP-STO is expected to respond to H_{MW}, as follows. Injection locking of the

magnetization of FGL or SIL occurs when the H_{MW} frequency (f_{MW}) is close to the intrinsic oscillation frequency. In contrast, no injection locking occurs when f_{MW} matches the difference frequency because there is no actual magnetization oscillation at this frequency. Based on this principle, we experimentally demonstrate that the multiple peaks in the STO signal can be assigned by examining injection locking. We also carry out micromagnetic simulations to investigate the magnetization dynamics of the STO during injection locking.

Figure 1(a) shows the structure of the sample and the experimental setup. The AIP-STO is a circular pillar fabricated from a polycrystalline giant magnetoresistive film consisting of FGL [FeCo (7 nm)], a spacer [Cu (5 nm)], and SIL [NiFe (3 nm)]. The pillar diameter is approximately 40 nm. An external field in the z direction (H_z) or the field tilted from the z direction toward the y direction by 23° (H_{ext}) was applied. A dc bias current (I_{STO}) was supplied to the STO in the direction from FGL to SIL. The STO signal was amplified and measured by a spectrum analyzer. Above the STO, a 100-nm-thick insulator layer and a waveguide were fabricated. By introducing an electrical signal from a signal generator to the waveguide, H_{MW} alternating in the x direction with the maximum frequency of 40 GHz was applied to the STO. The attenuation between the signal generator and the sample increases with frequency and is 3 dB at 40 GHz. Because of this attenuation, the H_{MW} amplitude was estimated to be 211 – 149 Oe and 297 – 211 Oe when the output power (P_{MW}) of the signal generator was set to +12 dBm or +15 dBm, respectively. The electrical signal used to generate H_{MW} leaked into the STO signal. The amplitude of this crosstalk was 0 dBm at the maximum and lower than the amplifier's 1-dB compression point of 7 dBm. Thus, the measurement of the STO signal was not disturbed by the crosstalk, despite that the crosstalk was much stronger than the STO signal.

Figure 1(b) shows the STO resistance versus H_z. At H_z = 0 Oe, the FGL and SIL magnetizations are in an antiparallel in-plane configuration due to the dipolar interaction. As H_z increases or decreases from zero, the FGL and SIL magnetizations tilt toward the + or $-z$ direction, and their configuration gradually becomes parallel. The resistance saturates at around H_z = ±8 kOe, showing that the FGL and SIL magnetizations are aligned in the $\pm z$ direction. Figure 1(c) shows the differential resistance versus I_{STO} for several H_z values from 6 kOe to 16 kOe. All the dV/dI curves exhibit a peak at I_{STO} < 1 mA. This peak is characteristic to the AIP-STO and corresponds to reversal of the SIL magnetization [10]. For H_z = 16 kOe, a dip appears as I_{STO} is further increased to 2.4 mA. The other dV/dI curves for smaller H_z also show undulations at similar I_{STO}. These changes in the dV/dI curves indicate the onset of magnetization oscillation.

We next present the power spectral density (PSD) of the STO signal. We first investigate the oscillation properties without H_{MW}. In the measurement of the STO signal, the field was tilted. According to the previous experimental studies of STO, tilting the field can cause more peaks to appear in the STO signal because of the distorted magnetization trajectory [7],[8],[10]. Since observing more peaks is advantageous for the analysis of the STO, we employed this technique. The amplifier gain was subtracted from the results.

Figure 2 shows the STO signal spectra versus H_{ext} obtained by supplying I_{STO} = 3 mA. There is a peak stretching from 10 GHz at H_{ext} = 5 kOe to 31 GHz at H_{ext} = 13 kOe with an almost linear frequency increase with respect to H_{ext}. This peak is referred to as the main peak, and its frequency is labeled f_{main}. The main peak becomes weak twice at around H_{ext} = 8 kOe and 10.5 kOe. In the H_{ext} range of 11–13 kOe, two additional peaks are observed, and their frequencies are labeled f_1 and f_2. These three peaks exhibit the frequency relation: $f_{\mathrm{main}} = f_1 + f_2$, suggesting

that either the f_1 or f_2 peak corresponds to the difference frequency. This is discussed later by using injection locking.

Figures 3(a)–3(d) show the STO signal spectra versus I_{STO} for H_{ext} = 7, 9.4, 10.9, and 12.5 kOe, respectively. The corresponding dV/dI curves are shown below the colormaps. All the dV/dI curves exhibit a peak at I_{STO} < 1 mA and are similar to those obtained in the perpendicular H_z [Fig. 1(c)]. This agreement suggests that the magnetization dynamics are fundamentally unchanged by tilting the external field. For H_{ext} = 7 kOe, the main peak is observed at around 14 GHz when I_{STO} = 3 mA, and this peak exhibits a frequency increase with respect to I_{STO} (blue-shift). For H_{ext} = 9.4 kOe, f_{main} increases to 21 GHz and similarly exhibits a blue-shift. There is also a broad signal in the low-frequency region below 5 GHz. For H_{ext} = 10.9 kOe, where the main peak disappears, only the low-frequency broad signal is observed. For H_{ext} = 12.5 kOe, the main peak appears again and exhibits a blue-shift saturating to 30 GHz. The f_1 peak also exhibits a blue-shift, whereas the f_2 peak exhibits a slight frequency decrease with respect to I_{STO} (red-shift). The main peak consistently exhibits the blue-shift for H_{ext} = 7, 9.4, and 12.5 kOe. Considering that the FGL and SIL oscillations are expected to exhibit blue- and red-shift, respectively, the main peak can be assigned to the oscillation frequency of FGL [10]–[12].

We next applied H_{MW} to investigate injection locking. Figures 4(a)–4(d) show the STO signal spectra versus f_{MW} for P_{MW} = 12 dBm and I_{STO} = 3 mA. The H_{ext} values are aligned with those in Figs 3(a)–3(d). At f_{MW} = 0 Hz, the STO signal spectra without H_{MW} are shown. In all the figures, the spectra without H_{MW} are basically the same as those with H_{MW} when f_{MW} is too low to affect the oscillation (for example at 1 GHz). This indicates that the temperature increase of the sample due to the electrical signal in the waveguide had little effect on the magnetization

oscillation.

For H_{ext} = 7 kOe, the main peak is affected by H_{MW} when f_{MW} is close to the intrinsic f_{main}. The inset shows the STO signal spectra for f_{MW} = 12.5–15 GHz at intervals of 0.5 GHz. For the f_{MW} range of 13–14.5 GHz, the peak moves to around f_{MW}, indicating that injection locking occurs. There is also a slight change in the main peak at f_{MW} = 29 GHz. This frequency corresponds to $f_{main} \times 2$, indicating that the oscillation is weakly affected when f_{MW} is twice the oscillation frequency.

For H_{ext} = 9.4 kOe, the injection locking similarly occurs when f_{MW} is close to the intrinsic f_{main} at around 21 GHz. The injection locking is also accompanied by the following two features in the low-frequency region: the low-frequency signal amplitude decreases at f_{MW} = 20 GHz and two peaks extend from the bottom axis at 21 GHz in both lower and higher frequency sides, creating a V-shape appearance. These features are also faintly observed for H_{ext} = 7 kOe [Fig. 4(a)]. The V-shape peaks are discussed later by using simulations.

For H_{ext} = 10.9 kOe, although the main peak is not observed, the low-frequency signal changes at f_{MW} = 25–30 GHz. This frequency roughly agrees with f_{main} estimated to be 26 GHz at H_{ext} = 10.9 kOe from the interpolation of the main peak in Fig. 2. This agreement suggests that magnetization oscillation may exist though it generates the STO signal too weak to measure.

For H_{ext} = 12.5 kOe, clear injection locking occurs when f_{MW} is close to the intrinsic f_{main}. Interestingly, the f_1 peak changes when the injection locking occurs to the main peak. In contrast, no change of the STO signal is observed when f_{MW} matches f_1. When f_{MW} is close to f_2, the f_2 peak itself does not exhibit any obvious change, but the weak V-shape peaks appear from the bottom axis at 24 GHz. These V-shape peaks are clearer in Fig. 4(f) obtained by increasing P_{MW}

to 15 dBm. By assuming that the V-shape peaks are indicative of the magnetization oscillation affected by H_{MW}, it is suggested that the f_2 peak corresponds to the actual magnetization oscillation. These results can be explained by assigning f_1 to the difference frequency. When injection locking occurs to the main peak and f_{main} follows f_{MW}, f_1 also changes because of the frequency relation between the peaks. No injection locking occurs for the f_1 peak because there is no actual magnetization oscillation at this frequency. This analysis demonstrates that the frequency of the actual magnetization oscillations and the difference frequency can be distinguished by examining injection locking. The main peak was already assigned to the FGL oscillation judging from the blue-shift in the I_{STO} dependence. However, the f_2 peak cannot be simply assigned to the SIL oscillation because its frequency is expected to be higher than that of the FGL oscillation, as explained below. When FGL and SIL is treated as a single magnetic layer by neglecting the interaction, the resonance frequency (f_{res}) of the magnetization with an oscillation cone angle (θ) is expressed as [14]

$$f_{\mathrm{res}} = \frac{\gamma}{2\pi}\left(H_z - 4\pi M_{\mathrm{s}}^{\mathrm{eff}} \cos\theta\right), \tag{1}$$

where γ is the gyromagnetic ratio, and $4\pi M_{\mathrm{s}}^{\mathrm{eff}}$ denotes the demagnetizing field determined by the saturation magnetization and the shape of the magnetic layer. Because θ of the SIL oscillation is more than 90° and θ of the FGL oscillation is less than 90°, the oscillation frequency of SIL is higher than that of FGL [10]–[12]. In fact, the experimental data reported in Ref. [10] support that the oscillation frequency of SIL is higher than that of FGL. The sample used in Ref. [10] has a thicker SIL (7 nm) and a smaller diameter (28 nm), and these differences might alter the oscillation behavior. Further study is required to fully elucidate the STO signal observed in this sample.

The STO signal spectra for f_{MW} = 27–33 GHz are shown in Fig. 4(e) at intervals of 1 GHz. In the locking range from 28 GHz – 32 GHz, no peaks are observed, suggesting that the STO signal

is confined at f_{MW} with the linewidth smaller than the resolution of the spectrum analyzer and hidden in the crosstalk signal, which is different from the Fig. 4(a) inset, where the peaks are still observed around f_{MW}. Figure 4(f) shows the data obtained under the same conditions as Fig. 4(d) except that P_{MW} is increased to 15 dBm. The result is basically the same with an increased locking range, as seen in the enlarged views in Figs. 4(g) and 4(h).

The magnetization dynamics of the AIP-STO under the application of H_{MW} was analyzed by micromagnetic simulations using the software *magnum.fe* [15]. This simulation code couples 3D magnetization dynamics and spin accumulation concurrently using the Landau–Lifshitz–Gilbert equation and spin-diffusion equations, as described in detail in the previous studies to evaluate the oscillation properties of AIP-STOs [10],[11]. The stacking structure of the simulation model is the same as the experimental sample. The diameter is set to 28 nm, which is smaller than the experimental sample and aligned with that used in the previous studies to facilitate the comparison of the results. A current density of 3×10^8 A/cm^2, a perpendicular H_z of 9 kOe, and H_{MW} of 100 Oe were applied. No thermal fluctuation field was taken into account

Figure 5(a) shows spectra of the FGL magnetization dynamics versus f_{MW} and the corresponding θ. Without H_{MW}, the frequency of the FGL oscillation (f_{FGL}) is approximately 10 GHz with θ around 61°. When f_{MW} is close to the intrinsic f_{FGL}, injection locking occurs, and the f_{FGL} peak follows f_{MW}, as seen in the inset. Below and above the locking range, the spectra exhibit two additional peaks higher and lower than f_{FGL} with the one matching f_{MW}. In the locking range, θ also changes. Based on Eq. (1), it can be interpreted that FGL adjust the oscillation frequency to follow f_{MW} by changing θ. Namely, when f_{MW} is lower (higher) than the intrinsic f_{FGL}, θ decreases (increases).

Figure 5(b) shows the spectra of the SIL magnetization dynamics versus f_{MW} and the

corresponding θ. Without H_{MW}, the frequency of the SIL oscillation (f_{SIL}) is approximately 35 GHz with θ around 120°. As already discussed, f_{SIL} is higher than f_{FGL} because of the larger θ. When f_{MW} = 10 GHz, f_{SIL} and θ change. This is because the change of the FGL magnetization due to the injection locking varies the spin-transfer torque from FGL to SIL and, consequently, affects the SIL oscillation. Around f_{MW} = 35 GHz, two additional peaks higher and lower than f_{SIL} weakly appear, which is similar to the case of FGL. This indicates that the SIL magnetization is affected by H_{MW}. The SIL oscillation is less susceptible to H_{MW} than the FGL oscillation presumably because of the smaller magnetic volume and higher oscillation frequency of SIL. The weak peak at around 10 GHz is attributed to the magnetization dynamics induced by the FGL oscillation through the dipolar and spin-transfer torque interactions. Thus, the f_{MW} dependence of this peak mimics that of the FGL oscillation.

Figure 5(c) shows the spectra of the electrical potential between the top and bottom of the STO versus f_{MW}, which qualitatively represents the STO signal. Because the external field is not tilted and the system is symmetric with respect to the z axis, the f_{FGL} and f_{SIL} peaks do not appear in the potential, and only the peak with a difference frequency (f_{MR}) at 25 GHz appears. Namely, the relation: $f_{\mathrm{MR}} = f_{\mathrm{SIL}} - f_{\mathrm{FGL}}$ holds. The result shows the following three features. When the injection locking occurs to the FGL oscillation, the f_{MR} peak changes because of the frequency relation. Injection locking does not occur when f_{MW} matches f_{MR}. V-shape peaks appear from the bottom axis at 10 GHz. These features qualitatively agree with the experimental results, supporting the discussion in the experimental part.

By closely looking at the experimental and simulation results, it is found that the V-shape peaks do not appear in the locking range and appear below and above the locking range. One difference

between the locking range and its vicinity is that the FGL magnetization dynamics shows a single peak or multiple peaks, as shown in Fig. 5(a). Furthermore, the interval between the multiple peaks matches the V-shape peak frequency. These facts imply that the magnetization dynamics with multiple frequency peaks has something to do with the origin of the V-shape peaks. The potential data exhibit several diagonal peaks other than the V-shape peaks. In relation to the diagonal peaks, we show the experimental result from another AIP-STO sample fabricated by the same procedure in Fig. 5(d). The result is basically same as Fig. 4(d), indicating the reproducibility of the experimental data, and an additional diagonal peak is observed, as designated by a dotted circle. Although the V-shape and diagonal peaks are reproduced by simulations, their origins are not fully understood and will be studied in future work

In summary, we analyzed the oscillation of an AIP-STO by applying an external H_{MW} and examining injection locking. The STO signal peaks corresponding to the oscillation frequency and the difference frequency were successfully distinguished based on the principle that injection locking occurs only to the peak corresponding to the magnetization oscillation. When the oscillation frequency was modified by the injection locking, the difference frequency also changed, which was consistent with their frequency relation. In addition, applying H_{MW} affected the signal in the low-frequency STO signal and gave rise to V-shape peaks. The magnetization dynamics under the application of H_{MW} were analyzed by micromagnetic simulations. The simulations confirmed that injection locking does not occur at the difference frequency, supporting the interpretation of the experimental results. The V-shape peaks were also reproduced by the simulations. These findings show that unique information provided by injection locking is useful for elucidating the oscillation of the AIP-STO and can contribute to the development of AIP-STOs for applications such as MAMR.

This work was partially supported by the Advanced Storage Research Consortium (ASRC), Japan and JSPS KAKENHI Grant Number JP19K05257.

REFERENCES

[1] J.-G. Zhu, X. Zhu, and Y. Tang, "Microwave assisted magnetic recording," IEEE. Trans. Magn. 44, 125 (2008).

[2] N. Narita, K. Yamada, T. Taguchi, T. Matsumoto, K. Koi, and A. Takeo, "Analysis of effective field gradient in microwave-assisted magnetic recording," IEEE Trans. Magn. 50, 3203004, (2014).

[3] S. Okamoto, N. Kikuchi, M. Furuta, O. Kitakami, and T. Shimatsu, "Microwave assisted magnetic recording technologies and related physics," J. Phys. D: Appl. Phys. 48, 353001 (2015).

[4] I. Tagawa, M. Shiimoto, M. Matsubara, S. Nosaki, Y. Urakami, and J. Aoyama, "Advantage of MAMR read-write performance," IEEE Trans. Magn. 52, 3101104 (2016).

[5] M. Takagishi, N. Narita, H. Iwasaki, H. Suto, T. Maeda, and A. Takeo, "Design concept of MAS effect dominant MAMR head and numerical study," IEEE Trans. Magn. vol. 57, 3300106 (2021).

[6] J.-G. Zhu and Y. Wang, "Microwave assisted magnetic recording utilizing perpendicular spin torque oscillator with switchable perpendicular electrodes," IEEE. Trans. Magn. 46, 751 (2010).

[7] H. Suto, T. Yang, T. Nagasawa, K. Kudo, K. Mizushima, and R. Sato, "Magnetization dynamics of a MgO-based spin-torque oscillator with a perpendicular polarizer layer and a planar free layer," J. Appl. Phys. 112, 083907 (2012).

[8] S. Bosu, H. Sepehri-Amin, Y. Sakuraba, S. Kasai, M. Hayashi, and K. Hono, "High frequency

out-of-plane oscillation with large cone angle in mag-flip spin torque oscillators for microwave assisted magnetic recording," Appl. Phys. Lett. 110, 142403 (2017).

[9] J.-G. Zhu, "Dual side spin transfer spin torque oscillator for microwave assisted magnetic recording," in Joint MMM-Intermag Conference 2016, San Diego, AB-11.

[10] W. Zhou, H. Sepehri-Amin, T. Taniguchi, S. Tamaru, Y. Sakuraba, S. Kasai, H. Kubota, and K. Hono, "Inducing out-of-plane precession of magnetization for microwave-assisted magnetic recording with an oscillating polarizer in a spin-torque oscillator," Appl. Phys. Lett. 114, 172403 (2019).

[11] H. Sepehri-Amin, W. Zhou, S. Bosu, C. Abert, Y. Sakuraba, S. Kasai, D. Suess, and K. Hono, "Design of spin-injection-layer in all-in-plane spin torque-oscillator for microwave assisted magnetic recording," J. Magn. Magn. Mater. 476, 361 (2019).

[12] T. Taniguchi, "Synchronized, periodic, and chaotic dynamics in spin torque oscillator with two free layers", J. of Magn. and Magn. Mater. 483, 281 (2019).

[13] S. Urazhdin, P. Tabor, V. Tiberkevich, and A. Slavin "Fractional synchronization of spin-torque nano-oscillators," Phys. Rev. Lett. 105, 104101 (2010).

[14] C. Kittel," On the theory of ferromagnetic resonance absorption," Phys. Rev. 73, 155 (1948).

[15] C. Abert, M. Ruggeri, F. Bruckner, C. Vogler, G. Hrkac, D. Praetorius, and D. Suess, "A three-dimensional spin-diffusion model for micromagnetics," Sci. Rep. 5, 14855 (2015).

FIG 1

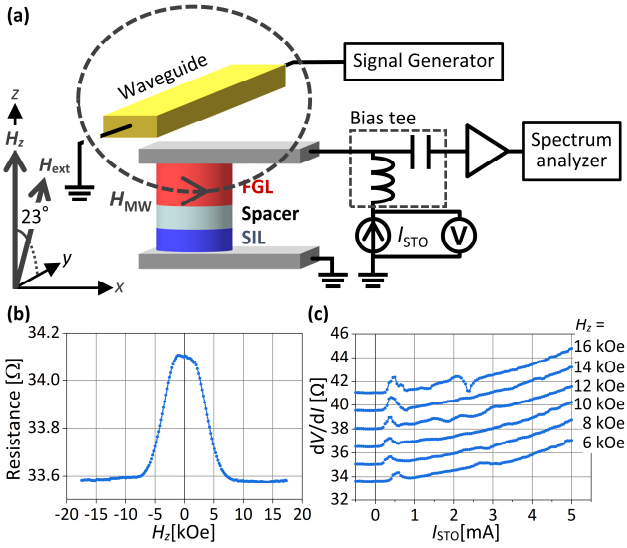

FIG. 1. (a) Schematic of the sample structure and measurement setup. (b) Sample resistance versus H_z obtained for $I_{STO} = 0.1$ mA. (c) dV/dI of the sample versus I_{STO} obtained for $H_z = 6$–16 kOe. Data are offset for clarity.

FIG 2

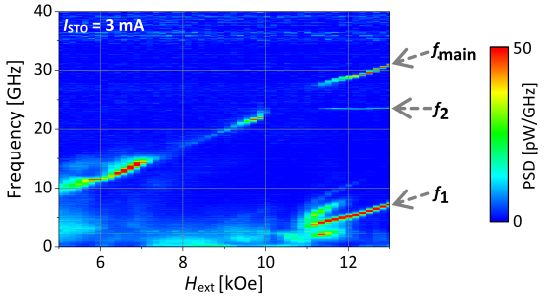

FIG. 2. PSD of the STO signal versus H_{ext} obtained for I_{STO} = 3 mA.

FIG 3

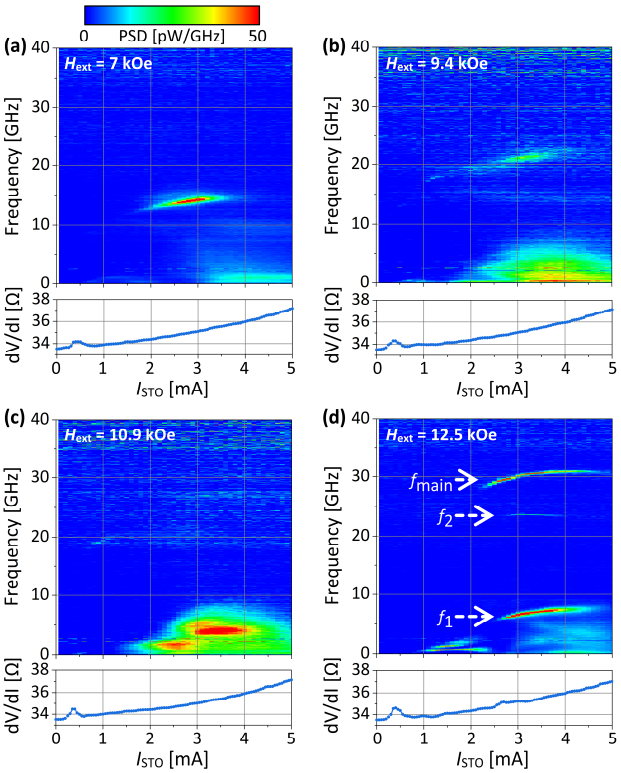

FIG. 3. PSD of the STO signal versus I_{STO} and the corresponding dV/dI curve obtained for H_{ext} = (a) 7 kOe, (b) 9.4 kOe, (c) 10.9 kOe, and (d)12.5 kOe. The scale at the top left is common to all colormaps. The color axis in (b) and (c) is magnified by a factor of 2.5.

FIG 4

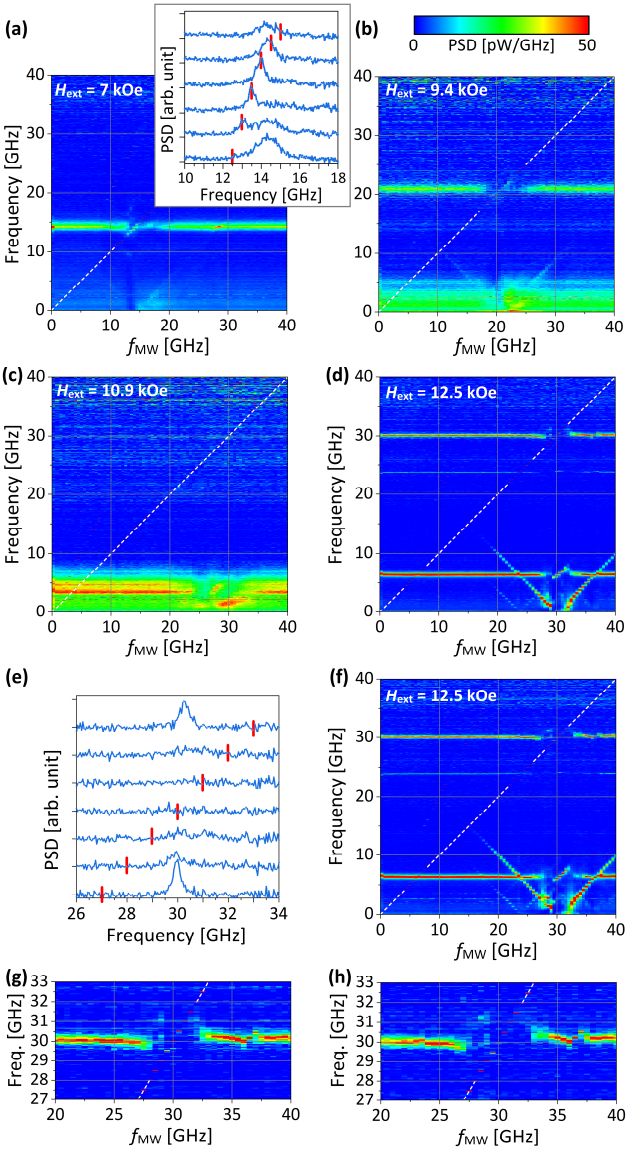

FIG. 4. PSD of the STO signal versus f_{MW} obtained for P_{MW} = 12 dBm; I_{STO} = 3 mA; and H_{ext} = (a) 7 kOe, (b) 9.4 kOe, (c) 10.9 kOe, and (d) 12.5 kOe. The scale at top right is common to all colormaps. The color axis in (b) and (c) is magnified by a factor of 2.5. The inset in (a) shows the line plot for f_{MW} = 12.5–15 GHz at intervals of 0.5 GHz. (e) Line plot of the result in (d) for f_{MW} = 27–33 GHz at intervals of 1 GHz. In the inset of (a) and in (e), data are offset for clarity, strong crosstalk is omitted for simplicity, and vertical bars represent f_{MW}. (f) PSD of the STO signal versus f_{MW} obtained for P_{MW} = 15 dBm, I_{STO} = 3 mA, and H_{ext} = 12.5 kOe. (g) and (h) Enlarged view of (d) and (f), respectively. The diagonal dashed lines represent the condition where the frequencies on the vertical and horizontal axes coincide.

FIG 5

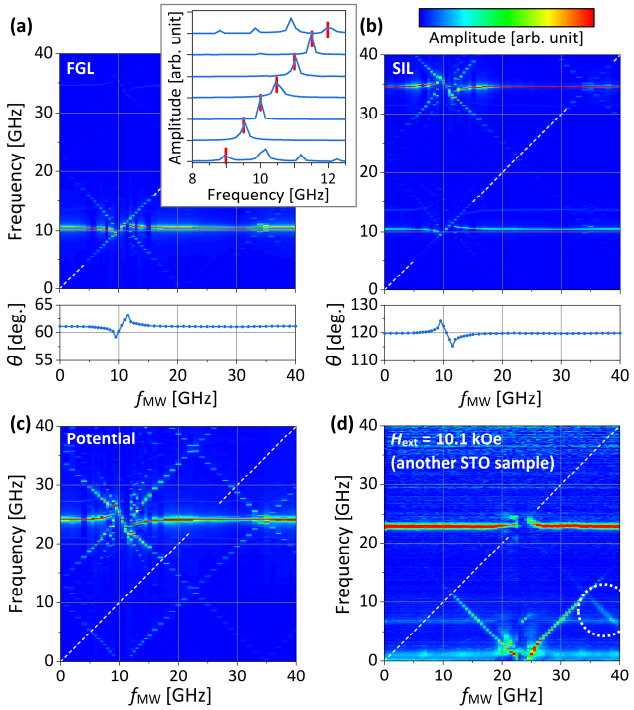

FIG. 5. Spectra of the computed x-component magnetization versus f_{MW} and the corresponding θ for (a) FGL and (b) SIL. The inset in (a) shows the line plot for f_{MW} = 9–12 GHz at intervals of 0.5 GHz. Data are offset for clarity and vertical bars represent f_{MW}. (c) Spectra of the computed potential versus f_{MW}. (d). PSD of the STO signal versus f_{MW} obtained from another experimental sample for P_{MW} = 12 dBm; I_{STO} = 4 mA; and H_{ext} = 10.1 kOe. The diagonal dashed lines represent the condition where the frequencies on the vertical and horizontal axes coincide.